Modeling magnetic fluctuations in the stripe ordered state

R. M. Konik,[1] F. H. L. Essler,[2] and A. M. Tsvelik[1]
[1]*Department of Condensed Matter Physics and Materials Science, Brookhaven National Laboratory, Upton, New York 11973-5000, USA*
[2]*The Rudolph Peierls Centre for Theoretical Physics, Oxford University, 1 Keble Road, Oxford OX1 3NP, United Kingdom*
(Received 16 July 2008; revised manuscript received 15 October 2008; published 16 December 2008)

In this work we study the magnetic behavior of a simple model of the stripe ordered phase of the cuprates, an array of alternating coupled doped and undoped two-leg Hubbard-type ladders. To obtain the coupled ladders' magnetic response, we employ available dynamical susceptibilities of the individual two-leg ladders and treat the interladder coupling in a random phase approximation. Strikingly, we find two possible scenarios for the ordered state induced by the coupling between ladders: the spin modulation may both occur in the conventional fashion, *perpendicular* to the direction of the stripes, but it may also occur *parallel* to the stripe direction. These two scenarios are differentiated according to different microscopic realizations of the component doped ladders. We argue that inelastic neutron scattering experiments on two stripe ordered cuprates, $La_{1.875}Ba_{0.125}CuO_4$ and $La_{2-x}Sr_xCuO_4$ at $x\sim 0.125$, do not readily distinguish between these scenarios due to manner in which stripes form in these materials.

DOI: 10.1103/PhysRevB.78.214509 PACS number(s): 71.10.Pm, 72.80.Sk

$La_{2-x}Ba_xCuO_4$ is the material where high-temperature superconductivity was first discovered by Bednorz and Müller in 1986.[1] At $x=0.125$ this material is defined by an anomalous suppression of T_c,[2] which has been argued[3–5] to be coincident with *static* stripe order, a unidirectional static charge and spin density wave. While there exist other cuprates exhibiting static stripe order, the most prominent being neodymium-doped $La_{1.6-x}Nd_{0.4}Sr_xCuO_4$ (LSCO),[6] there exists a wider class of allied compounds possessing "dynamic stripes," a phenomenon characterized by short-range charge-density wave (CDW) order and incommensurate low- (but finite) energy magnetic excitations. While their presence or absence in any given material is controversial, dynamic stripes can be argued to be seen in both $YBa_2Cu_3O_{6+x}$ (Refs. 7–11) and in $La_{2-x}Sr_xCuO_4$.[12,13]

Magnetic order associated with the stripe phase appears in two different guises in these copper oxides. In neutron measurements on untwinned crystals of $YBa_2Cu_3O_{6.6}$ exactly *two* incommensurate low-energy peaks are seen.[8,9] Observations of the phonon anomaly in this material are contradictory, with initial measurements suggesting that the magnetic peaks are displaced from the wave vector (π,π) along a direction *perpendicular* to the stripes,[14] while later measurements of the same anomaly[15] arguing the displacement is *parallel* to the stripes. The origin of magnetic order in $La_{1.875}Ba_{0.125}CuO_4$ and $La_{2-x}Sr_xCuO_4$ is similarly ambiguous but for different reasons. In these materials, *four* peaks in the neutron scattering intensity are observed. This doubling in the number of peaks corresponds to a doubling of the unit cell in the La-based materials. Each cell spans two copper-oxide planes where the stripes in each plane are orientated at 90° relative to one another. This doubling obscures the relative orientation of the magnetic relative to the charge order. In $La_{1.875}Ba_{0.125}CuO_4$ this doubling occurs as part of its LTT structure, while in $La_{2-x}Sr_xCuO_4$ the doubling can only be dynamically present in its corresponding LTO structure.

Despite this ambiguity, it is widely believed, based upon the observed charge incommensuration as a function of doping, x, that magnetic order arises perpendicular to the charge stripe order. However, as we will argue, this evidence is not dispositive, at least for $x\sim 1/8$. Synonymously, we will also demonstrate that the ordering is not theoretically constrained. To this end we present a model where magnetic ordering may arise equally naturally perpendicular or parallel to the stripe direction.

The model we study, originally suggested for $x=1/8$ doped LBCO by Tranquada *et al.*,[4] begins by treating a single copper-oxide plane as an array of coupled two-leg Hubbard-type ladders, where the unit cell contains one undoped (U) and one doped (D) two-leg ladder. In the model it is the presence of the doped two-leg ladders that permits two scenarios for magnetic ordering to arise. One scenario is favored over the other on the basis of particular nonuniversal features in the spin response of an individual doped ladder.[16] This nonuniversality then implies that at least in the context of our model, one scenario is not fundamentally more natural than the other.

An important ancillary consequence that flows from our model is a natural explanation for the π phase shift concomitant with the incommensurate magnetic order. In models where the doped striped regions are treated as magnetically inert voids,[17–19] the undoped parts of the copper-oxide plane are connected via effective *ferromagnetic* couplings so that the correct incommensurate order is produced. Instead here, we show that a model of *antiferromagnetically* connected doped and undoped ladders is able to produce the π-phase shift.

A fundamental assumption underlying the model we are analyzing is that stripes are not merely a low-energy phenomenon but rather exist over a large range of energies. Support for this view may be derived from inelastic neutron scattering experiments,[4,20,21] where a strong inelastic signal between 50 and 100 meV has been attributed to arise from stripe correlations. However, it is not yet fully understood (but see Refs. 22–25) how to reconcile such a stripe-based picture with the existence of nodal quasiparticles established in angle-resolved photoemission data.[26] And while stripe correlations may exist at higher energies, they are certainly not isolated phenomena. Typically, higher energy inelastic neu-

 ©2008 The American Physical Society

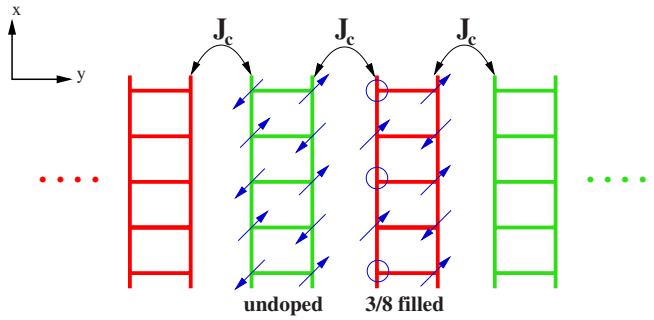

FIG. 1. (Color online) A schematic of an alternating infinite array of coupled half-filled and doped ladders. We take the coupling J_c to be antiferromagnetic.

tron scattering observations[4,21] only see broad features, indicating at the least, strong damping.

While our model pertains primarily to magnetic order at 1/8 doping, where the incommensurate ordering wave vector approximately[3] equals $Q_s=\pi(1\pm 1/4,1)$ or $Q_s=\pi(1,1\pm 1/4)$, it is also capable of describing other values of incommensuration. In the second scenario of ordering presented below, the incommensuration results from the position of the low-lying quasicoherent mode on the doped ladder, which is itself a linear function of doping. While this requires the assumption that that doping adds holes to the stripe without changing the distance between stripes, it is perhaps a useful step toward a description of the striped phase in $La_{2-x}Sr_xCuO_4$ for $0.055<x<0.125$, where parallel stripe order appears with incommensuration linear in x.

While we do not address directly the origin of superconductivity, a particularly attractive feature of this model is that superconductivity arises naturally from the strong pairing correlations present in doped ladders.[27–30] In order to judge the applicability of such a model it is first important to analyze its implications for the magnetic dynamics of the striped phase. This is the aim of the present paper.

I. MODEL

The basic model underlying our calculations is illustrated in Fig. 1: we have an array of alternating doped and undoped Hubbard-type ladders.[31] The charge gap in the undoped ladders is taken to be large. As a result the dominant interaction between ladders is antiferromagnetic superexchange J_c. As is clear from the above discussion, the experimentally observed charge order with approximate commensurate wave vector[3,32]

$$\mathbf{Q}_c=\left(0,\pm\frac{\pi}{2}\right) \tag{1}$$

is built into our model. The issue we want to address is the static spin order that develops upon coupling the ladders together, as well as the spin dynamics. While it is widely believed that magnetic long-range order develops at

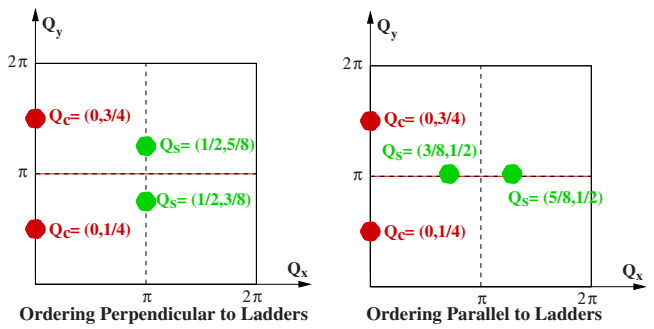

FIG. 2. (Color online) Two possible scenarios for magnetic and charge long-range order in the coupled ladder model. The wave vectors are marked in units of 2π.

$$\mathbf{Q}_s=\left(\pi,\pi\pm\frac{\pi}{4}\right), \tag{2}$$

that is, perpendicular to the stripes, we want to suggest an alternative scenario where the magnetic long-range order develops *along* the direction of the stripes, i.e.,

$$\mathbf{Q}_s=\left(\pi\pm\frac{\pi}{4},\pi\right). \tag{3}$$

The two scenarios are illustrated in Fig. 2.

II. ANALYSIS OF THE MAGNETIC RESPONSE

The basic ingredients of our approach are dynamical susceptibilities of the two types of ladders. As our subsequent analysis is based on a random phase approximation (RPA) in the interladder couplings, this is the only information required. It turns out that the results obtained in such an approach display a certain robustness with respect to changing the microscopic details of the model. This allows us to identify prominent features of the magnetic response, which we believe to be insensitive of the particular approximations we employ.

The dominant interladder coupling is taken to be antiferromagnetic superexchange of strength J_c (see Fig. 1), which is induced by virtual hopping processes between doped and undoped ladders. The matrix susceptibilities for the U and D ladders are expressed in terms of the matrices

$$M_{\mathrm{U}}(\omega,q_x,q_y)=\begin{pmatrix}\chi_{11}^{\mathrm{ud}}(\omega,q_x) & e^{iq_ya}\chi_{12}^{\mathrm{ud}}(\omega,q_x)\\ e^{-iq_ya}\chi_{21}^{\mathrm{ud}}(\omega,q_x) & \chi_{22}^{\mathrm{ud}}(\omega,q_x)\end{pmatrix},$$

$$M_{\mathrm{D}}(\omega,q_x,q_y)=\begin{pmatrix}\chi_{11}^{\mathrm{d}}(\omega,q_x) & e^{iq_ya}\chi_{12}^{\mathrm{d}}(\omega,q_x)\\ e^{-iq_ya}\chi_{21}^{\mathrm{d}}(\omega,q_x) & \chi_{22}^{\mathrm{d}}(\omega,q_x).\end{pmatrix}, \tag{4}$$

via

$$\chi_a(q_x,q_y,\omega)=\mathrm{Tr}\,M_a\cdot K,\quad a=\mathrm{U},\mathrm{D}, \tag{5}$$

where K is defined by

$$K=\begin{pmatrix}1 & 1\\ 1 & 1\end{pmatrix}. \tag{6}$$

Here $\chi_{11}=\chi_{22}$ marks correlations along the legs of the ladder, while $\chi_{12}=\chi_{21}$ describes correlations of the ladder rungs.

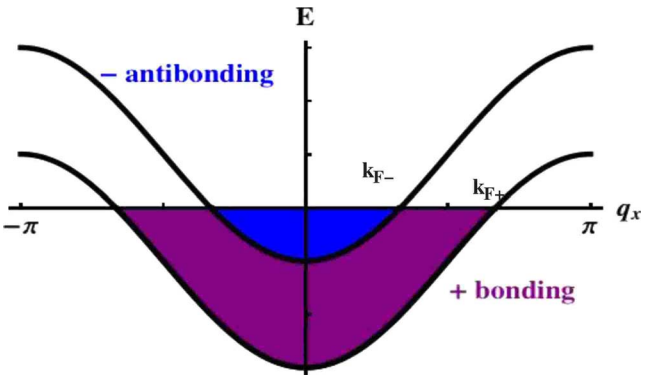

FIG. 3. (Color online) Band structure of Hubbard-type ladders. ± denote bonding and antibonding bands, respectively, and the chemical potential generically leads to partial filling of both bands.

The coupling between the ladders is then taken into account in RPA. In the matrix notation introduced above this amounts to

$$\chi_{2D}^{RPA}(\omega,q_x,q_y) = \mathrm{Tr}[(1+M_D J)M_U(1-JM_D JM_U)^{-1}K]$$

$$+ \mathrm{Tr}[(1+M_U J)M_D(1-JM_U JM_D)^{-1}K], \quad (7)$$

where J is a matrix given by

$$J = \begin{pmatrix} 0 & e^{-iq_y a}J_c \\ e^{iq_y a}J_c & 0 \end{pmatrix}. \quad (8)$$

The scattering function for the coupled ladders is then $S(q_x,q_y,\omega) \sim -\mathrm{Im}\ \chi_{2D}^{RPA}(\omega,q_x,q_y)$.

Long-range magnetic ordering occurs when $\chi^{2D}(\omega=0,q_x,q_y)$ develops a singularity at some Q_x and Q_y. In the RPA the development of the singularity is equivalent to the vanishing of $\mathrm{Det}(1-JM_U JM_D)$, which gives

$$0 = (1-J_c^2\chi_{11}^d\chi_{11}^{ud})^2 + J_c^4[(\chi_{12}^d\chi_{12}^{ud})^2 - (\chi_{12}^d\chi_{11}^{ud})^2 - (\chi_{11}^d\chi_{12}^{ud})^2]$$
$$- 2J_c^2\chi_{12}^d\chi_{12}^{ud}\cos(4q_y). \quad (9)$$

In the above, both χ_{ij}^d and χ_{ij}^{ud} are functions of only q_x and ω, while q_y only appears in the final cosine.

Ultimately the RPA approximation we employ for short-ranged couplings between ladders is uncontrolled. The approximation can, however, be turned into a controlled expansion if interladder interactions are treated as long ranged.[33] In presenting RPA results for $\chi^{2D}(\omega=0,q_x,q_y)$ we will always work with a coupling strength, J, just below J_c. If so desired, it is unproblematic to employ the RPA approximation directly in the ordered phase.[34] It however changes none of our results on qualitative level.

Once we have the doped and undoped ladder susceptibilities in hand, we will readily be able to determine the value of the transverse wave vector, q_y, at which order arises. We will find two scenarios, one with order at $q_y=\pi\pm\pi/4$, and one with order at $q_y=\pi$. One of our main conclusions is that which scenario is realized depends on the details of the ladder susceptibilities.

III. LADDER SUSCEPTIBILITIES: GENERAL STRUCTURE

A. Susceptibility of the undoped ladders

The low-energy spectral weight of the undoped ladders is concentrated around $q_x=q_y=\pi$, and the susceptibility displays a modulation along the y direction by the factor $[1-\cos(q_y)]$.[35] As long as we restrict our attention to energies below the two magnon continuum (which dominates the response at $q_y=0$), we can express the susceptibilities of the undoped ladders in the form

$$\chi_{ab}^{ud}(\omega,q_x) = \chi^{ud}(\omega,q_x)\begin{pmatrix} 1 & -1 \\ -1 & 1 \end{pmatrix}_{ab}, \quad (10)$$

where

$$\chi^{ud}(\omega,q_x) = \frac{Z(q_x)}{\omega^2-\epsilon^2(q_x)}. \quad (11)$$

The magnon dispersion relation, $\epsilon(q_x)$, is taken from Ref. 36,

$$\epsilon(q_x) = J\{[1.89\cos(q_x/2)]^2 + [0.507\sin(q_x/2)]^2$$
$$+ [1.382\sin(q_x)]^2\}^{1/2}. \quad (12)$$

The residue $Z(q_x)$ can be inferred from Ref. 37. We use the following simple, approximate fit, $Z(q_x)=3J[0.65\sin^2(q_x/2)+0.27]$.

B. Susceptibility of the doped ladders

In order to infer the susceptibilities of the doped ladders it is useful to recall the band structure. There are two bands corresponding to bonding (+) and antibonding (−) fermions, respectively, $c_{\pm,\sigma}=(c_{1,\sigma}\pm c_{2,\sigma})/\sqrt{2}$. Generically both bands will cross the chemical potential, leading to four Fermi wave numbers $-k_{F\pm}$ and $k_{F\pm}$ as is illustrated in Fig. 3. The mapping to the bonding and antibonding picture implies the following decomposition of the doped susceptibilities χ_{ab}^d:

$$\chi_{ab}^d(\omega,q_x) = \chi_{\mathrm{intra}}^d(\omega,q_x) + \chi_{\mathrm{inter}}^d(\omega,q_x)\begin{pmatrix} 1 & -1 \\ -1 & 1 \end{pmatrix}_{ab}. \quad (13)$$

Here $\chi_{\mathrm{intra}}^d(\omega,q_x)$ and $\chi_{\mathrm{inter}}^d(\omega,q_x)$ denote the parts of the susceptibility involving only fermions within the same band and fermions of both bands, respectively.

The band structure further dictates that low-energy spin excitations occur at $q_x\approx 0,\pm 2k_{F+},\pm 2k_{F-}$ in χ_{intra}^d and at $q_x\approx\pm k_{F+}\mp k_{F-},\pm k_{F+}\pm k_{F-}$ in χ_{inter}^d, respectively. At low energies, we therefore can write

$$\chi_{\mathrm{intra}}^d(\omega,q_x) = \chi_0^d(\omega,q_x) + \chi_{2k_{F+}}^d(\omega,q_x) + \chi_{2k_{F-}}^d(\omega,q_x), \quad (14)$$

$$\chi_{\mathrm{inter}}^d(\omega,q_x) = \chi_{k_{F+}+k_{F-}}^d(\omega,q_x) + \chi_{k_{F+}-k_{F-}}^d(\omega,q_x). \quad (15)$$

Here the single-magnon weight (though only quasicoherent due to the gapless charge excitations of the doped ladder) is found in $\chi_{k_{F+}+k_{F-}}^d$. The remaining contributions represent two excitation continua.

IV. ORIGIN OF MAGNETIC INSTABILITY

In terms of the interband and intraband susceptibilities of the doped ladders the RPA instability condition [Eq. (9)] reads

$$1 = 4J_c^2\chi^{\rm ud}(\omega,q_x)[\sin^2(2q_y)\chi^{\rm d}_{\rm intra}(\omega,q_x) + \cos^2(2q_y)\chi^{\rm d}_{\rm inter}(\omega,q_x)]. \quad (16)$$

This form makes it obvious that there are three possible sources for a magnetic instability: it can be driven by (1) the interband susceptibility of the doped ladders, $\chi^{\rm d}_{\rm inter}(\omega,q_x)$; (2) the intraband susceptibility of the doped ladders, $\chi^{\rm d}_{\rm intra}(\omega,q_x)$; or finally, (3) by the susceptibility of the undoped ladder, $\chi^{\rm ud}(\omega,q_x)$. In the first case the ordering occurs at $q_y=\pi\pm\frac{\pi}{4}$, in the second case at q_y mod $\pi=0,\frac{\pi}{2}$ and in the final case at $q_y=\pi$.

In this first scenario, the ordering occurs at

$$\mathbf{Q}_s^I = \left(\pi,\pi\pm\frac{\pi}{4}\right). \quad (17)$$

Here the ordering arises from predominance of the two-particle scattering continuum over the single-particle magnon. In this scenario, the specific form of the doped susceptibilities, based upon treating the doped ladders as a manifestation of the SO(6) Gross-Neveu model, are given in Appendix.

In the second scenario the ordering occurs at

$$\mathbf{Q}_s^{II} = [\pm(k_{F+}+k_{F-}),\pi]. \quad (18)$$

Here the ordering arises from the spectral weight associated with the single-particle magnon on the doped ladder, found near wave vector $D=k_{F+}+k_{F-}$. (For 1/8-doped LBCO, $D=\frac{3\pi}{4}$.) In this scenario this spectral weight overwhelms that of the two-particle continuum in the doped ladders [as encoded in $\chi^{\rm d}_{\rm intra}(\omega,q_x)$]. To then treat this case, we imagine that the susceptibility of the doped ladder comes solely from the single-particle magnon as discussed in further detail in the Appendix.

In the third and final scenario, the ordering occurs at the commensurate wave vector

$$\mathbf{Q}_s^{III} = (\pi,\pi). \quad (19)$$

Here the ordering arises because the spectral weight of the undoped ladder dominates. It is however the least relevant scenario for describing neutron scattering experiments on the cuprates and so will not be explored in detail here.

V. MAGNETIC RESPONSE OF COUPLED LADDERS

We now elaborate upon the magnetic response of the coupled ladders in the two scenarios presented in the previous section. In particular we will show that either of these scenarios is compatible with the observed gross features of the magnetic response of $La_{1.875}Ba_{0.125}CuO_4$ and $La_{2-x}Sr_xCuO_4$.

We first consider constant energy slices of the spin response as a function of wave vector.[31] Choosing the same energies reported in Ref. 4, we plot the results in Figs. 5 and 6, where the reduced lattice units h and k are defined via[4]

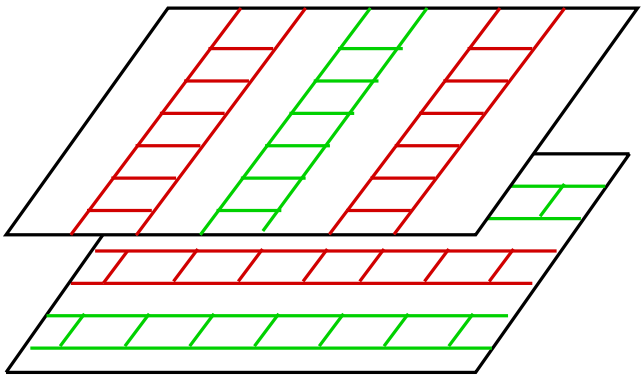

FIG. 4. (Color online) Stacking of planes of ladders.

$$h=\frac{q_x+q_y}{2\pi},\quad k=\frac{q_y-q_x}{2\pi}. \quad (20)$$

In both figures we show the spin response resulting for a single plane of ladders (left figure of each pair) and for a pair of planes of ladders orientated at 90° to one another (right figure of each pair). The second arrangement (pictured in Fig. 4) corresponds to how stripes order in $La_{1.875}Ba_{0.125}CuO_4$ and $La_{1.82}Sr_{0.18}CuO_4$, and so is the one relevant for comparison with experiment. We, however, include the response of a single plane as it is here that the magnetic responses of the two ordering scenarios most sharply distinguish themselves.

In Fig. 5, Scenario I is presented, the case where the magnetic order develops perpendicular to the ladder, i.e., at wave vector $(\pi,\pi\pm\frac{\pi}{4})$. At the lowest of energies shown, $\omega=6$ meV, we find for a single plane of ladders, a pair of incommensurate spin waves dispersing at the incommensurate wave vectors $(h,k)=(1\pm1/8,\pm1/8)$. In the response for two planes, we then observe a second pair of spin waves, rotated by 90° relative to the first. The dispersions cones of the wave vectors are elongated along the diagonal, a consequence of the anisotropy between inter- and intra-ladder-couplings (J_c and J). As we increase in energy to $\omega=36$ meV, the spin waves disperse outwards. We see that spectral weight of the cones is anisotropically distributed, with more weight being found on the side of the cone nearest to (π,π). Thus we see that as we increase in energy, the spectral weight appears to move away from the incommensurate points toward (π,π). By $\omega=55$ meV, the energy corresponding to the gap in the undoped ladders, the cones have begun to overlap. This overlap is enhanced for the response of a pair of planes, leading to the most intense response coming from (π,π). As energy is further increased, we observe a rotation in the intensity by 45° in the pair plane response (compare energies $\omega=36$ meV and $\omega=80$ meV). The rotation results from the dominance of the spin response of the half-filled ladders, which for a single plane form lines of intensity. With a pair of relatively orientated planes, the lines cross, leading to the four peaks. As we increase energy further, the peaks in the two-plane response disperse out-

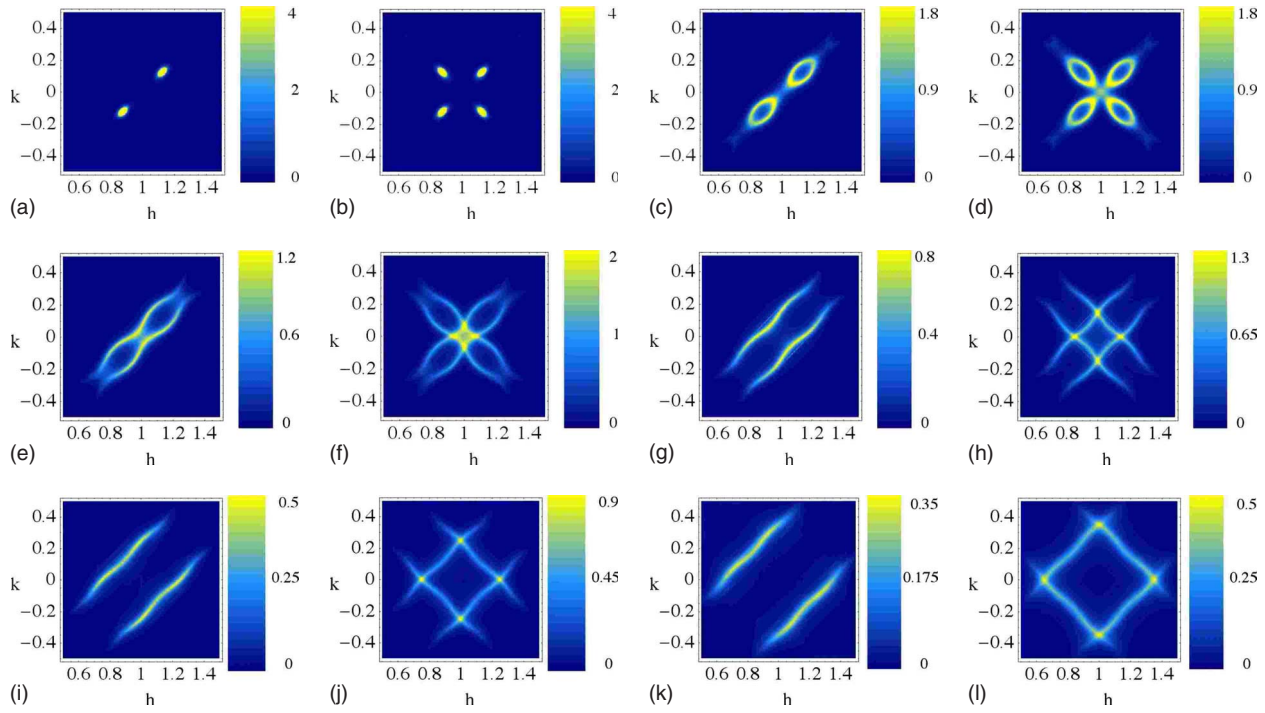

FIG. 5. (Color online) Plots of the scattering intensity in ordering Scenario I as a function of h and k (reduced lattice units) for a number of energies. At each energy the response is presented for both a single ladder array (left-hand figure) and two ladders arrays orientated at 90° relative to one another (right-hand figure). The parameters employed here are discussed in Appendix A1.

wards while at the same time losing intensity. By $\omega = 160$ meV, the spin response has become both comparatively broad and weak.

Of the two scenarios, the first scenario most strongly resembles previous spin-wave computations.[17–19] In particular the similarity between Fig. 5 of the text and Fig. 3 of Ref. 18 and Fig. 3 of Ref. 17 is striking. The similarity necessarily arises as in all cases ordering is taking place perpendicular to the ladders. In our second scenario, ordering is driven by the low-lying spin mode in the doped ladders, a feature absent from the spin-wave models.

In Fig. 6, we plot the magnetic response of the second scenario where order appears parallel to the ladders. At the lowest energy shown, $\omega = 6$ meV, we again find incommensurate spin waves, which now appear, for a single plane, at $(h,k) = (1 \mp 1/8, \pm 1/8)$. The spin waves, in this case, are much more strongly anisotropic. But we believe this is a feature of the details of the ladder susceptibilities, not a fundamental feature of the model. While the response at $\omega = 6$ meV for this ordering pattern is rotated by 90° relative to where the order develops perpendicular to the ladders, the response for a pair of planes is qualitatively no different in the two cases. As we increase in energy, the spin waves appearing at low energies evolve into the response of a set of nearly uncoupled doped ladders. Accompanying this evolution is a separate development of spectral weight at (π, π). The presence of inelastic spectral weight of (π, π) is a consequence of the competition in this scenario between order developing at $q_x = \pi$ (the location of coherent mode on the doped ladder) and order developing incommensurately at $q_x = 3\pi/4$ and $5\pi/4$ (the location of the quasicoherent mode on the undoped ladder). Though in this case order is favored at the incommensurate wave vector, the commensurate order remains pre-emergent and so appears at finite energy values. Taken together, these two effects again give the appearance of a movement of spectral weight toward (π, π). As we continue further up in energy, the response of the half-filled ladders again begins to dominate, with a peak in the intensity near (π, π) (see $\omega = 55$ meV in Fig. 6). The dominance of the half-filled ladders then continues to higher energies ($\omega = 80$ meV and above), and consequently, the response takes on the same form as that of Fig. 5.

While our model of coupled ladders finds reasonable approximates to the observations on LBCO of Ref. 4, it produces features at higher energies that are typically much sharper than those actually observed. This however is not surprising. The RPA approximation we employ will generically underdamp high-energy stripelike correlations.

As another measure of the response of the two scenarios, we compute at fixed energy the q-integrated intensity, $S(\omega)$, of the coupled ladders. This quantity is defined by

$$S(\omega) = \int d^2q \ \mathrm{Im}\ \chi(\omega, q_x, q_y). \tag{21}$$

We plot the results in Fig. 7 for the two scenarios. We see we obtain a rough agreement. At low energies there is an increase in intensity corresponding to the development of incommensurate long-range order. We also see an enhancement in the intensity at $J = 50$ meV, which corresponds to the spin gap of the half-filled ladders. This is to be expected as the excitation spectrum of the half-filled ladder is a single coherent mode and should have a strong response. For energies in excess of the spin gap, we then see a gradual decline

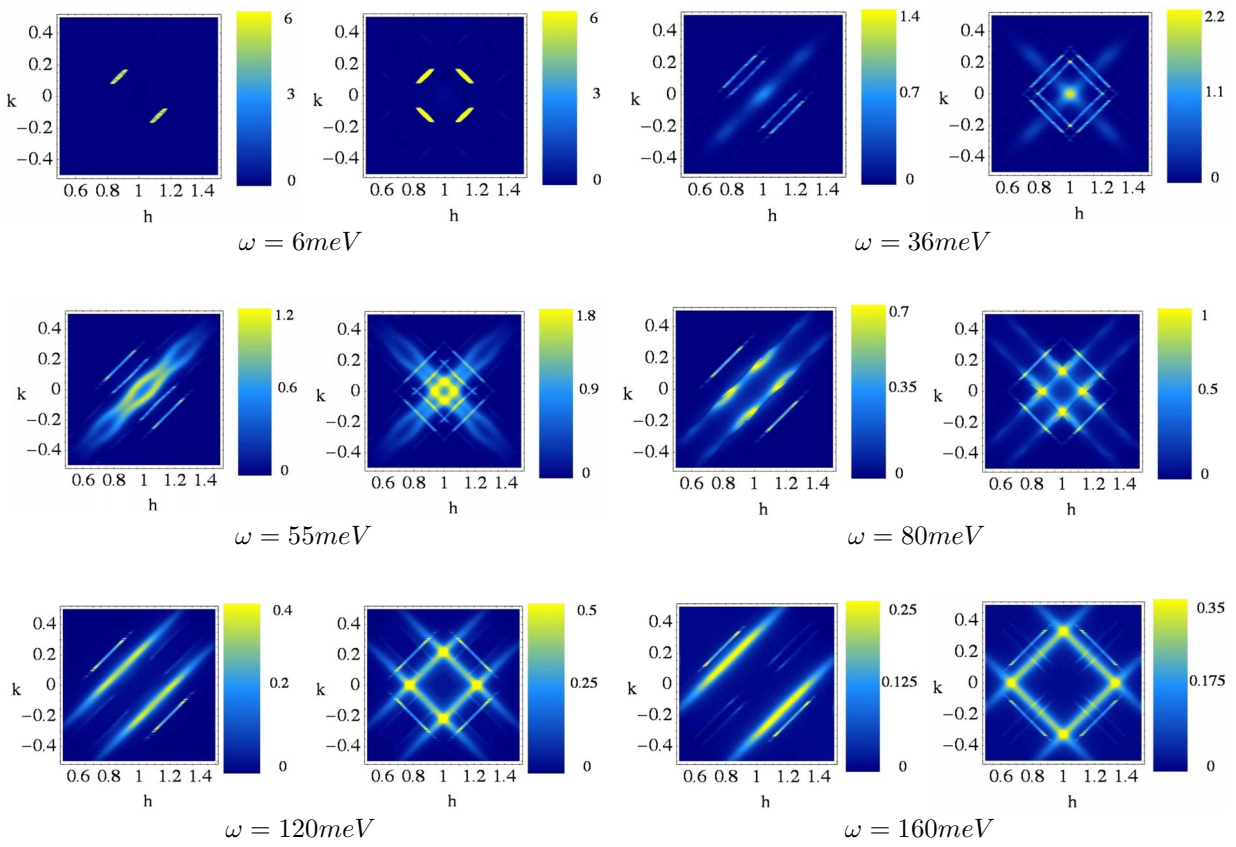

FIG. 6. (Color online) Plots of the scattering intensity in ordering Scenario II as a function of h and k (reduced lattice units) for a number of energies. The presentation scheme is the same as Fig. 5. The parameters for the ladders used here are discussed in Appendix A2.

in intensity in both the measured and computed responses. The primary difference between the two scenarios lies in the total amount of spectral weight found at low energies. But this difference is not fundamental and rather is a product of particular choices made to describe the susceptibilities of the individual ladders in both cases.

VI. DISCUSSION

The observations of Refs. 3 and 4 of the inelastic spin response in $La_{1.875}Ba_{0.125}CuO_4$ has several basic features. At zero energy there appear inelastic incommensurate spin waves at approximately the four wave vectors, $Q=[\pi,\pi(1\pm 1/4)]$ and $Q=[\pi(1\pm 1/4),\pi]$. At small but finite energies (up to 50 meV), the intensity associated with these spin waves appears to propagate inwards away from these incommensurate points toward (π,π). At higher energies, the movement of the spectral weight reverses direction, propagating outward, but with peaks rotated by 45° relative to the low-energy spin waves.

While both coupled ladder scenarios qualitatively reproduce these features, there are quantitative differences between scenarios. The low-energy spectral features present in Scenario II (ordering along the ladder) are far more anisotropic than those in Scenario I (ordering perpendicular to the ladder). This however is less a fundamental feature of Scenario II and more a consequence of the use of the field theoretic treatment of the doped ladders at medium energies. At such energies, the neglected nonrelativistic band curvature will moderate anisotropic features. A more fundamental difference is the manner in which spectral weight moves inwards toward (π,π) as energies are increased to 50 meV. In Scenario I, this movement is a consequence of expanding spin-wave cones possessing an unequal distribution of spectral weight. In Scenario II, the weight moves toward (π,π) due to the spectral features present on the uncoupled doped ladder together with nascent ordering at (π,π) [see Scenario III of Sec. IV].

Although the primary focus of this work has been on static stripe order of the kind observed in $La_{1.875}Ba_{0.125}CuO_4$, one may ask whether our model of coupled ladders might be applicable more generally to incommensurate magnetic excitations in the cuprates, a question of considerable theoretical interest.[38] At least to some degree it does. In slightly overdoped LSCO ($La_{1.84}Sr_{0.16}CuO_4$), nascent incommensurate long-range order has been reported.[39–41] Specifically, neutron scattering experiments observe a broad peak centered about 11 meV in the scattering intensity at the incommensurate wave vector $(h,k)=(1\pm 1/8,\pm 1/8)$ (see Fig. 8). (A similar phenomena is seen in $La_{1.82}Sr_{0.18}CuO_4$.[42]) This magnetic response can be understood through our model of ladders with an interladder coupling, J_c, less than its critical ordering value, $J_{\rm crit}$. The responses for $J_c<J_{\rm crit}$ for both scenarios ($\parallel$ and $\perp$) are pictured in Fig. 8. For comparison we have plotted the corresponding responses for $J_c=J_{\rm crit}$, where long-range order is fully developed. There, as ω is decreased, the

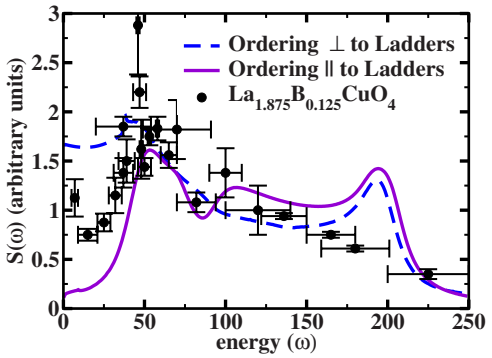

FIG. 7. (Color online) Integrated intensity, $S(\omega)$, of the coupled ladder system in the two ordering scenarios. For comparison, we plot these results against Ref. 4. The parameters are the same as for Figs. 5 and 6.

response diverges at the incommensurate wave vector.

Experimental evidence beyond the spin response in these compounds provides only limited evidence, allowing one to distinguish between these two scenarios. In Scenario I extended to general levels of doping,[43] incommensurate wave vectors of charge and spin density waves are arranged perpendicular to the direction of stripes and are related to each other via

$$\mathbf{Q}_{ch}^{\mathrm{I}} = (0, \pm 4\pi x), \quad \mathbf{Q}_{s}^{\mathrm{I}} = (\pi, \pi \pm 2\pi x), \tag{22}$$

where x denotes the doping. In contrast, in Scenario II, stripes are found in the form of coupled two-leg ladders, independent of doping, gaining in this fashion, magnetic energy. Here the pattern of incommensuration appears as

$$\mathbf{Q}_{ch}^{\mathrm{II}} = \left(0, \pm \frac{\pi}{2}\right), \quad \mathbf{Q}_{s}^{\mathrm{II}} = (\pi \pm 2\pi x, \pi). \tag{23}$$

The behavior of incommensurate spin order at $Q_{sx} = \pi \pm 2\pi x$ as a function of doping directly tracks the wave vector where low-energy quasicoherent modes exist in the doped ladder.

To distinguish between these two scenarios we must then focus upon the charge incommensuration. However only the doping dependence of the magnetic incommensuration has been carefully studied (see Ref. 20 and references therein). The experiments show that the spin incommensuration is proportional to the doping x for $x < 1/8$ and then saturates. On the other hand charge peaks have been observed only for a narrow range of dopings and only in stripe-stabilized cuprates [in $La_{1.5}Nd_{0.4}Sr_{0.1}CuO_4$,[44] $La_{1.475}Nd_{0.4}Sr_{0.125}CuO_4$,[45] $La_{1.45}Nd_{0.4}Sr_{0.15}CuO_4$,[46] and $La_{1.875}Ba_{0.125}CuO_4$ (Ref. 5)]. While the observed charge incommensuration, Q_{ch}, changes as a function of x [and so is supportive of Scenario I], it does so weakly, i.e., the change in Q_{ch} is governed by $\delta Q_{\mathrm{ch}} = c\,\delta x$ with $c \sim 0.5$.[20] One might then want to conclude that Scenario II remains a possibility, at least for dopings in a narrow window about $x \sim 0.125$. The situation is similarly ambiguous for $YBa_2Cu_3O_{6+x}$. Here distinct measurements of the phonon anomaly support alternatively Scenario I (Refs. 8 and 9 and Scenario II.[15]

Independent of either scenario, our modeling efforts, in the limited context of models of coupled Hubbard-type ladders, show the value of taking into account the doped region of the copper-oxide planes. In coupling together the ladders, we employed *antiferromagnetic* couplings but were nonetheless able to explain the appearance of incommensurate order and the corresponding π-phase shift in magnetic order. If the doped regions were instead considered inert, a *ferromagnetic* coupling would have to be assumed between adjacent doped ladders.[17–19,47] While it is important to take the doped regions into account, it is of course no surprise that once done the π-phase shift is found. It has long been understood that the π-phase shift is a concomitant feature of holes localized into stripelike regions.[48–51]

While we have focused on magnetism here, models of coupled ladders have promising superconducting properties.[52] It has already been established that a model of a uniform array of coupled half-filled ladders possesses narrow

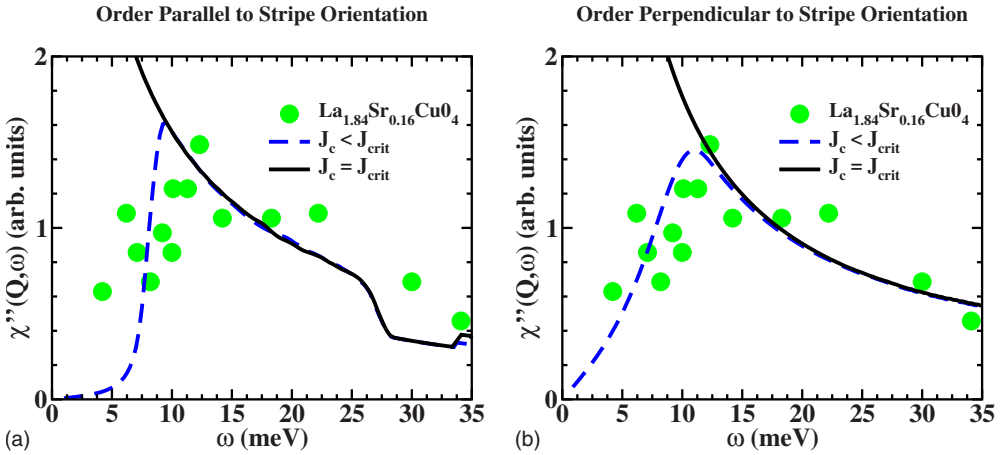

FIG. 8. (Color online) The intensity of the spin response at the incommensurate ordering wave vector, Q, for the two ordering scenarios. We show the response for both subcritical and critical values of the interladder coupling, J_c. We compare this with the maximal intensity in $La_{1.84}Sr_{0.16}CuO_4$ for $T > T_c$ measured in Ref. 40. For ordering perpendicular to the ladders the parameters are the same as those found in Figs. 5 and 7. For the second scenario, as explained in Appendix A2, the parameters used differed from those employed in Figs. 6 and 7.

arcs of quasiparticles, which have an instability toward d-wave superconductivity.[30] Ultimately this is a consequence of the presence of nascent d-wave superconducting order on the component ladders.[27,28] However these arcs are highly anisotropic with an alignment parallel to the ladders. Can then the present model produce arcs aligned at 45°? If so it would provide an important complement to initial theoretical efforts[22–25] on how to understand the presence of nodal quasiparticles seen in angle-resolved photoemission experiments[26] in the context of a stripe-based picture.

ACKNOWLEDGMENTS

This work was supported by the EPSRC under Grant No. GR/R83712/01 (F.H.L.E.), the U.S. DOE under Contract No. DE-AC02-98 CH 10886 (A.T. and R.M.K.). F.H.L.E. acknowledges the support from Theory Institute for Strongly Correlated and Complex Systems at BNL and NSF under Contract No. DMR 0240238. We are grateful to J. Tranquada for discussions and interest in the work.

APPENDIX: SUSCEPTIBILITIES OF THE DOPED LADDERS

We extract the susceptibilities of doped ladder from a field theoretic reduction of the ladders (Ref. 53). The corresponding field theory takes the form of the SO(6) Gross-Neveu model supplemented by a U(1) Luttinger liquid describing the charge sector. Though such a description captures low-energy features of the system, it leaves us with ambiguities concerning the amplitudes of the correlation functions. It is these ambiguities which give rise to the possibility of different ordering scenarios described in the text.

The field theory predicts the following general form for the susceptibilities:

$$\chi_0^{\mathrm{d}}(\omega,q)=\frac{3}{8}A_{11}J_1(\omega,q),$$

$$\chi_{2k_{F+}}^{\mathrm{d}}(\omega,q)=\frac{3}{8}A_{12}[J_2(\omega,q+2K_{F+})+J_2(\omega,q-2K_{F+})],$$

$$\chi_{2k_{F-}}^{\mathrm{d}}(\omega,q)=\frac{3}{8}A_{12}[J_2(\omega,q+2K_{F-})+J_2(\omega,q-2K_{F-})],$$

$$\chi_{k_{F+}-k_{F-}}^{\mathrm{d}}(\omega,q)=\frac{3}{8}A_{31}[J_1(\omega,q+K_{F-}-K_{F+})+J_1(\omega,q-K_{F-}+K_{F+})],$$

$$\chi_{k_{F+}+k_{F-}}^{\mathrm{d}}(\omega,q)=\frac{3}{8}A_{32}[J_3(\omega,q+K_{F-}+K_{F+})+J_3(\omega,q-K_{F-}-K_{F+})]. \tag{A1}$$

In these expressions A_{ij} are amplitudes with dimensionality of momentum that are determined by short-distance physics. On the other hand J_i's are functions dependent on long-distance physics that arise from the form of the matrix elements of the spin operators in the $SO(6)$ Gross-Neveu model. Different choice of the amplitudes, A_{ij}, determine what ordering scenario is realized.

The imaginary part of J_1 takes the form

$$\mathrm{Im}\,J_1(\omega,q)=\frac{8v_F\tilde{q}^2}{(\omega^2-\tilde{q}^2)^{3/2}}\frac{\theta(\omega-\sqrt{\tilde{q}^2+4m^2})}{(\omega^2-\tilde{q}^2-4m^2)^{1/2}}\times\exp\left\{\int_0^\infty\frac{dx}{x}\frac{G_c(x)}{s(x)}\left[1-c(x)\cos\left(\frac{\theta_{12}x}{\pi}\right)\right]\right\}, \tag{A2}$$

where θ_{12} is given by

$$\theta_{12}=\cosh^{-1}\left(\frac{\omega^2-\tilde{q}^2-2m^2}{2m^2}\right), \tag{A3}$$

and $\tilde{q}=v_Fq$, where v_F is the Fermi velocity of electrons in either the bonding or antibonding bands. Here $s(x)/c(x)\equiv\sinh(x)/\cosh(x)$ and

$$G_c(x)=\frac{e^{x/2}-1}{s(x)}.$$

The imaginary parts of J_2 and J_3 can be expressed more compactly as integrals over hypergeometric functions,

$$J_2(\omega,q)=\frac{v_F}{m^2}\int_{-\infty}^{\infty}d\theta\frac{s^2(\theta)}{[c(\theta)]^{4-K/2}}F\left(1-\frac{K}{4},1-\frac{K}{4},1,\frac{(\omega+i0)^2-\tilde{q}^2}{4m^2c^2(\theta)}\right)\times\exp\left\{\int_0^\infty\frac{dx}{x}\frac{G_s(x)}{s(x)}\left[1-c(x)\cos\left(\frac{2\theta x}{\pi}\right)\right]\right\},$$

$$J_3(\omega,q)=\frac{v_F}{2g^2m^2}\exp\left[-2\int_0^\infty\frac{dx}{x}\frac{G_v(x)}{s(x)}s^2\left(\frac{x}{4}\right)\right]\times F\left[1-\frac{K}{4},1-\frac{K}{4},1,\frac{(\omega+i0)^2-\tilde{q}^2}{2m^2}\right]+\frac{2^{K/4}v_F}{\pi m^2}\int_{-\infty}^{\infty}d\theta\frac{1}{[c(\theta)]^{4-K/2}}\left[\frac{s(2\theta)^2}{2c(2\theta)^2}+\frac{s(\theta)^2}{c(2\theta)^2}\right]\times F\left[1-\frac{K}{4},1-\frac{K}{4},1,\frac{(\omega+i0)^2-\tilde{q}^2}{4m^2c^2(\theta)}\right]\times\exp\left\{\int_0^\infty\frac{dx}{x}\frac{G_v(x)}{s(x)}\left[1-c(x)\cos\left(\frac{2\theta x}{\pi}\right)\right]\right\}, \tag{A4}$$

where

$$G_v(x)=\frac{2}{1-e^{-2x}}[e^{-2x}(1-e^{x/2})-e^{-5x/2}(1-e^{2x})].$$

Here K is the Luttinger parameter governing the gapless total charge mode of the doped ladder, and g is a constant given by

$$g^2 = \frac{2\sqrt{\pi}\Gamma(7/4)}{3\Gamma(5/4)}.$$

To evaluate the real parts of J_a $(a=1,2,3)$ we Kramers-Kronig transform the above expressions for Im J,

$$\text{Re } J(\omega,q) = \frac{1}{\pi}\int_{-D}^{D} d\omega' \frac{\text{Im } J(\omega',q)}{\omega-\omega'}. \tag{A5}$$

We equip the transformation with a cutoff, $D \sim v_F/a$, to reflect the fact the imaginary parts of J_2 and J_3 are only accurate representations of the low-energy sector of the ladders. To determine the real parts of $J_{2/3}$ we perform the transformation over a frequency interval roughly corresponding to this sector. Our results, however, are insensitive to the exact value of D.

1. Scenario I: Ordering perpendicular to the ladders

To be able to produce the analysis of ordering perpendicular to the ladders [Scenario I—Figs. 5, 7, and 8] we had to fix the parameters $v_F A_{ij}/m^2$ and determine the value of spin gap m. In Ref. 53, we did this through a comparison with an RPA analysis of a Hubbard ladder with an onsite U repulsion. The value of the spin gap m is related to the bandwidth, t, the Hubbard interaction, U, and the Fermi velocity v_F. For $t \approx U$ we chose $t=4$ eV and for $v_F=350$ meV a (where a is the lattice spacing). v_F is not readily available as its (strong) renormalization due to interactions is a two-loop effect. But the value we employed is commensurate with what is measured in the cuprates.[54] As discussed in Ref. 53, knowledge of t alone is enough to fix the value of the gap, $m=26$ meV, using a field theory analysis for doped ladders[55] together with the values of the gap on the ladder as determined from density matrix renormalization group (DMRG) at half-filling.[56,57] From this same field theory analysis, the Luttinger parameter can be determined as $K=0.945$. In Figs. 5 and 7 we couple the ladders together with a strength just below that of the critical interladder coupling as determined from our RPA analysis—here $J_{\text{crit}}=16.05$ meV. We choose the value of J on the undoped ladders to be 100 meV so as to match experimental observations of the location of the neck of the hourglass describing the evolution of excitations in $La_{1.875}Ba_{0.125}CuO_4$.[4] Furthermore to partially mimic the broadening seen in experiment, we broadened the spectral function of the undoped ladders by assuming a lifetime of $0.1J$.

The constants, A_{ij}, that appear in Eq. (A1) are not determined by the field theory treatment itself but must be accessed through separate considerations. In Ref. 53 we, through a comparison with a RPA analysis of a Hubbard ladder with an onsite U repulsion, were able to provide tentative values for the A_{ij}'s.

2. Scenario II: Ordering parallel to the ladders

Since the amplitudes A_{ij} are determined by processes with energies of the order of the bandwidth, we have a liberty of choice. For Scenario I we have chosen the high-energy physics as in a simple doped Hubbard ladder with a pointlike interaction and $U \sim t$. One can imagine that some other lattice realization generates a set of amplitudes such that the spectral weight associated with the quasicoherent spin excitation dominates. To develop this scenario, we thus focus on this excitation to the exclusion of contributions coming from two excitation scattering continua. Specifically we set $A_{11}=A_{12}=A_{31}=0$, leaving only A_{32} finite, and take J_3 to equal

$$J_3(\omega,k) = \frac{v_F}{2g^2m^2}\exp\left[-2\int_0^\infty \frac{dx}{x}\frac{G_v(x)}{\sinh(x)}\sinh^2\left(\frac{x}{4}\right)\right] \times F\left(1-\frac{K}{4},1-\frac{K}{4},1,\frac{\omega^2-\tilde{k}^2}{2m^2}\right). \tag{A6}$$

As such, J_3 now represents a coherent mode broadened by the presence of gapless charge excitations.

For this scenario, in order to produce the spin response at constant energy in Fig. 6 and the integrated intensity in Fig. 7, we must choose the ratio of v_f/m to be sufficiently large in order to guarantee Scenario II prevails over Scenario III. To ensure this we chose $v_f=250$ meV a, and the lattice bandwidth to be $t=1000$ meV (and thus via Refs. 55–57, $m=0.0065t=6.5$ meV). Both the parameters used for the undoped ladder and the Luttinger parameter describing charge excitations on the doped ladders were the same as in Scenario I (Appendix A1).

In order to produce the results displayed in the left-hand side of Fig. 8 (discussing the strength of the inelastic signal in $La_{1.86}Sr_{0.14}CuO_4$ at the incommensurate wave vector), we took instead $v_f=360$ meV a and $t=3000$ meV. This in turn moved the gap scale on the doped ladders to $m=21$ meV, high enough so that it did not interfere with the low-energy signal marking nascent incommensurate order.

[1] J. G. Bednorz and K. A. Müller, Z. Phys. B: Condens. Matter **64**, 189 (1986).

[2] A. R. Moodenbaugh, Y. Xu, M. Suenaga, T. J. Folkerts, and R. N. Shelton, Phys. Rev. B **38**, 4596 (1988).

[3] M. Fujita, H. Goka, K. Yamada, J. M. Tranquada, and L. P. Regnault, Phys. Rev. B **70**, 104517 (2004).

[4] J. M. Tranquada, H. Woo, T. G. Perring, H. Goka, G. D. Gu, G. Xu, M. Fujita, and K. Yamada, Nature (London) **429**, 534 (2004).

[5] P. Abbamonte, A. Rusydi, S. Smadici, G. D. Gu, G. A. Sawatzky, and D. L. Feng, Nat. Phys. **1**, 155 (2005).

[6] Stripe phases are also found in allied compounds to the cuprates, for example the nickelates, $La_{2-x}Sr_xNiO_{4+\delta}$. See, for example J. M. Tranquada, D. J. Buttrey, V. Sachan, and J. E. Lorenzo, Phys. Rev. Lett. **73**, 1003 (1994).

[7] P. Dai, H. A. Mook, R. D. Hunt, and F. Doğan, Phys. Rev. B **63**, 054525 (2001).

[8] H. A. Mook, P. Dai, F. Doğan, and R. D. Hunt, Nature (London) **404**, 729 (2000).

[9] V. Hinkov, S. Pailhès, P. Bourges, Y. Sidis, A. Ivanov, A. Kulakov, C. T. Lin, D. P. Chen, C. Bernhard, and B. Keimer, Nature (London) **430**, 650 (2004).

[10] V. Hinkov, P. Bourges, S. Pailhs, Y. Sidis, A. Ivanov, C. D. Frost, T. G. Perring, C. T. Lin, D. P. Chen, and B. Keimer, Nat. Phys. **3**, 780 (2007).
[11] V. Hinkov, D. Haug, B. Fauqué, P. Bourges, Y. Sidis, A. Ivanov, C. Bernhard, C. T. Lin, and B. Keimer, Science **319**, 597 (2008).
[12] K. Yamada, C. H. Lee, K. Kurahashi, J. Wada, S. Wakimoto, S. Ueki, H. Kimura, Y. Endoh, S. Hosoya, G. Shirane, R. J. Birgeneau, M. Greven, M. A. Kastner, and Y. J. Kim, Phys. Rev. B **57**, 6165 (1998).
[13] M. Fujita, K. Yamada, H. Hiraka, P. M. Gehring, S. H. Lee, S. Wakimoto, and G. Shirane, Phys. Rev. B **65**, 064505 (2002).
[14] See Ref. 8 above for evidence to this effect. We do note however that Ref. 15 has reported observations of this same phonon anomaly indicating that the incommensurate spin modulation is found along the stripes.
[15] L. Pintschovius, W. Reichardt, M. Kläser, T. Wolf, and H. v. Löhneysen, Phys. Rev. Lett. **89**, 037001 (2002).
[16] In particular, the low-energy field theoretic treatment that we employ to characterize the spin response of the doped ladder does not uniquely fix the real part of the susceptibility, a quantity dependent upon high-energy nonuniversal physics.
[17] M. Vojta and T. Ulbricht, Phys. Rev. Lett. **93**, 127002 (2004).
[18] G. S. Uhrig, K. P. Schmidt, and M. Grüninger, Phys. Rev. Lett. **93**, 267003 (2004).
[19] D. X. Yao, E. W. Carlson, and D. K. Campbell, Phys. Rev. B **73**, 224525 (2006); D. X. Yao and E. W. Carlson, *ibid.* **77**, 024503 (2008).
[20] J. M. Tranquada, in *Handbook of High-Temperature Superconductivity*, edited by J. R. Schrieffer and J. S. Brooks (Springer, New York, 2005).
[21] Guangyong Xu, J. M. Tranquada, T. G. Perring, G. D. Gu, M. Fujita, and K. Yamada, Phys. Rev. B **76**, 014508 (2007); We also note that a model of coupled ladders with alternating doping was studied in Ref. 25 (see below), but there the emphasis was understanding the origin of superconductivity.
[22] M. Granath, V. Oganesyan, S. A. Kivelson, E. Fradkin, and V. J. Emery, Phys. Rev. Lett. **87**, 167011 (2001); M. Granath, V. Oganesyan, D. Orgad, and S. A. Kivelson, Phys. Rev. B **65**, 184501 (2002).
[23] M. Vojta, Phys. Rev. B **78**, 144508 (2008); H. Weber and M. Vojta, *ibid.* **77**, 125118 (2008).
[24] M. Granath, Phys. Rev. B **77**, 165128 (2008).
[25] E. Berg, C.-C. Chen, and S. A. Kivelson, Phys. Rev. Lett. **100**, 027003 (2008).
[26] T. Valla, A. V. Fedorov, J. Lee, J. C. Davis, and G. D. Gu, Science **314**, 1914 (2006); M. R. Norman, A. Kanigel, M. Randeria, U. Chatterjee, and J. C. Campuzano, Phys. Rev. B **76**, 174501 (2007).
[27] M. Fabrizio, Phys. Rev. B **48**, 15838 (1993).
[28] H.-H. Lin, L. Balents, and M. P. A. Fisher, Phys. Rev. B **58**, 1794 (1998).
[29] E. Arrigoni, E. Fradkin, and S. A. Kivelson, Phys. Rev. B **69**, 214519 (2004).
[30] R. M. Konik, T. M. Rice, and A. M. Tsvelik, Phys. Rev. Lett. **96**, 086407 (2006).
[31] While we take as our starting point regions of segregated doping, for arguments governing the energetics of stripe formation see S. R. White and D. J. Scalapino, Phys. Rev. Lett. **80**, 1272 (1998); A. L. Chernyshev, S. R. White, and A. H. Castro Neto, Phys. Rev. B **65**, 214527 (2002); M. Bosch and Z. Nussinov, arXiv:cond-mat/0208383 (unpublished); see also, Refs. 48–50 as well as V. J. Emery, S. A. Kivelson, and H. Q. Lin, Phys. Rev. Lett. **64**, 475 (1990); U. Löw, V. J. Emery, K. Fabricius, and S. A. Kivelson, Phys. Rev. Lett. **72**, 1918 (1994).
[32] Y.-J. Kim, G. D. Gu, T. Gog, and D. Casa, Phys. Rev. B **77**, 064520 (2008).
[33] F. H. L. Essler and A. M. Tsvelik, Phys. Rev. B **65**, 115117 (2002).
[34] F. H. L. Essler, A. M. Tsvelik, and G. Delfino, Phys. Rev. B **56**, 11001 (1997).
[35] S. Notbohm, P. Ribeiro, B. Lake, D. A. Tennant, K. P. Schmidt, G. S. Uhrig, C. Hess, R. Klingeler, G. Behr, B. Büchner, M. Reehuis, R. I. Bewley, C. D. Frost, P. Manuel, and R. S. Eccleston, Phys. Rev. Lett. **98**, 027403 (2007).
[36] T. Barnes and J. Riera, Phys. Rev. B **50**, 6817 (1994).
[37] K. P. Schmidt and G. S. Uhrig, Mod. Phys. Lett. B **19**, 1179 (2005).
[38] M. Vojta, T. Vojta, and R. K. Kaul, Phys. Rev. Lett. **97**, 097001 (2006).
[39] B. Lake, G. Aeppli, T. E. Mason, A. Schröder, D. F. McMorrow, K. Lefmann, M. Isshiki, M. Nohara, H. Takagi, and S. M. Hayden, Nature (London) **400**, 43 (1999).
[40] N. B. Christensen, D. F. McMorrow, H. M. Rønnow, B. Lake, S. M. Hayden, G. Aeppli, T. G. Perring, M. Mangkorntong, M. Nohara, and H. Tagaki, Phys. Rev. Lett. **93**, 147002 (2004).
[41] B. Vignolle, S. M. Hayden, D. F. McMorrow, H. M. Rønnow, B. Lake, C. D. Frost, and T. G. Perring, Nat. Phys. **3**, 163 (2007).
[42] J. M. Tranquada, C. H. Lee, K. Yamada, Y. S. Lee, L. P. Regnault, and H. M. Rønnow, Phys. Rev. B **69**, 174507 (2004).
[43] O. Zachar, S. A. Kivelson, and V. J. Emery, Phys. Rev. B **57**, 1422 (1998).
[44] T. Niemöller, N. Ichikawa, T. Frello, H. Hünnefeld, N. H. Andersen, S. Uchida, J. R. Schneider, and J. M. Tranquada, Eur. Phys. J. B **12**, 509 (1999).
[45] J. M. Tranquada, B. J. Sternlieb, J. D. Axe, Y. Nakamura, and S. Uchida, Nature (London) **375**, 561 (1995)
[46] N. Ichikawa, S. Uchida, J. M. Tranquada, T. Niemöller, P. M. Gehring, S.-H. Lee, and J. R. Schneider, Phys. Rev. Lett. **85**, 1738 (2000).
[47] F. Krüger and S. Scheidl, Phys. Rev. B **67**, 134512 (2003).
[48] J. Zaanen and O. Gunnarsson, Phys. Rev. B **40**, 7391 (1989).
[49] H. J. Schulz, J. Phys. (France) **50**, 2833 (1989).
[50] K. Machida, Physica C **158**, 192 (1989).
[51] O. Zachar, Phys. Rev. B **65**, 174411 (2002).
[52] K.-Y. Yang, T. M. Rice, and F.-C. Zhang, Phys. Rev. B **73**, 174501 (2006).
[53] F. H. L. Essler and R. M. Konik, Phys. Rev. B **75**, 144403 (2007).
[54] R. Coldea, S. M. Hayden, G. Aeppli, T. G. Perring, C. D. Frost, T. E. Mason, S.-W. Cheong, and Z. Fisk, Phys. Rev. Lett. **86**, 5377 (2001).
[55] R. Konik, F. Lesage, A. W. W. Ludwig, and H. Saleur, Phys. Rev. B **61**, 4983 (2000).
[56] E. Jeckelmann, D. J. Scalapino, and S. R. White, Phys. Rev. B **58**, 9492 (1998).
[57] Z. Weihong, J. Oitmaa, C. J. Hamer, and R. J. Bursill, J. Phys.: Condens. Matter **13**, 433 (2001).